JPP Journal of Pharmacy and Pharmacology

JPP 2008, 60: 1049–1060

Received October 18, 2007
Accepted January 19, 2008
DOI 10.1211/jpp.60.8.0011
ISSN 0022-3573

Assessment of tissue redox status using metabolic responsive contrast agents and magnetic resonance imaging

Fuminori Hyodo, Benjamin P. Soule, Ken-ichiro Matsumoto, Shingo Matusmoto, John A. Cook, Emi Hyodo, Anastasia L. Sowers, Murali C. Krishna and James B. Mitchell

Abstract

Regulation of tissue redox status is important to maintain normal physiological conditions in the living body. Disruption of redox homoeostasis may lead to oxidative stress and can induce many pathological conditions such as cancer, neurological disorders and ageing. Therefore, imaging of tissue redox status could have clinical applications. Redox imaging employing magnetic resonance imaging (MRI) with nitroxides as cell-permeable redox-sensitive contrast agents has been used for non-invasive monitoring of tissue redox status in animal models. The redox imaging applications of nitroxide electron paramagnetic resonance imaging (EPRI) and MRI are reviewed here, with a focus on application of tumour redox status monitoring. While particular emphasis has been placed on differences in the redox status in tumours compared to selected normal tissues, the technique possesses the potential to have broad applications to the study of other disease states, inflammatory processes and other circumstances where oxidative stress is implicated.

Introduction

In-vivo molecular imaging research is an emerging discipline in medical research (Margolis et al 2007) and there has been considerable progress especially in the development of small animal imaging research (Koo et al 2006). Computed tomography (CT), positron emission tomography (PET), single photon emission computed tomography (SPECT), magnetic resonance imaging (MRI) and optical imaging are being used to visualize patho/pysiological conditions non-invasively (Herholz et al 2007; Torigian et al 2007). One of the prevalently used molecular imaging techniques is 18-fluorodeoxyglucose (FDG) with PET technique (Hoh 2007). MRI and PET have allowed clinicians to correlate anatomic abnormalities with biochemical attributes to better identify metastatic lesions. Such non-invasive imaging techniques can provide better and more patient-specific treatment since therapy can be tailored to the disease specifically (Huzjan et al 2005; Herholz et al 2007; Hoh 2007).

The redox environment (Schafer & Buettner 2001) within the tumour cell is an important parameter that may determine the response of a tumour to certain chemotherapeutic agents, radiation and bio-reductive hypoxic cell cytotoxins (Yu & Brown 1984; Mitchell & Russo 1987; Stratford et al 1994). A variety of intracellular molecules may contribute to the overall redox status in tissues, including glutathione (GSH), thioredoxins, NADPH, flavins, ascorbate and others (Schafer & Buettner 2001). Collectively, the reducing species may have an impact on how a particular tissue responds to oxidative stress induced by a particular drug or treatment modality and, therefore, a non-invasive means of determining the redox status of a tissue should be a useful adjunct for clinical oncology. In addition, breakdown of redox balance may lead to oxidative stress and can induce many pathological conditions, such as cancer, neurological disorders and ageing (Halliwell & Gutteridge 1999). Therefore, imaging of tissue redox status and monitoring the antioxidant level could be useful potentially in the diagnosis of disease states and in the assessment of treatment response in the case of cancer. Electron paramagnetic resonance imaging (EPRI) is an imaging modality which detects unpaired electrons in such species as transition metal complexes and free

Radiation Biology Branch, Center for Cancer Research, National Cancer Institute, NIH, Bethesda, MD, USA

Fuminori Hyodo,
Benjamin P. Soule,
Ken-ichiro Matsumoto,
Shingo Matusmoto,
John A. Cook, Emi Hyodo,
Anastasia L. Sowers,
Murali C. Krishna,
James B. Mitchell

Correspondence: J. B. Mitchell, Building 10, Room B3B69, NIH, Bethesda, MD 20892-1002. E-mail: jbm@HELIX.NIH.GOV

Funding: This work was supported by the intramural research program of the Center for Cancer Research, National Cancer Institute, NIH.

radicals, and using magnetic field gradients, provides spatial distribution of free radicals (Kuppusamy et al 1994; Liu et al 1995; Subramanian et al 2004). Free radicals are present at extremely low levels in tissue, below the detection limits of EPR. Whereas this was initially felt to be a limitation to the use of this technique in biological imaging, it was quickly discovered that agents containing unpaired electrons, or agents converted to such a compound in-vivo, could be introduced into a living system and detected using frequencies similar to those used in magnetic resonance imaging (MRI). This review focuses on the application of redox imaging for tumour redox status using EPRI or MRI and redox-sensitive contrast agents.

Nitroxides as antioxidants and redox probes

Stable nitroxide free radicals and their one-electron reduced products, namely the hydroxylamines, are recycling antioxidants (Soule et al 2007). By undergoing one-electron transfer reactions, nitroxides are reduced to the corresponding hydroxylamines or oxidized to the corresponding oxoammonium cation species (Figure 1). Therefore, nitroxides are redox-active species, which can be oxidized or reduced by the corresponding reactants in cells and tissues. Once administered in-vivo, all three forms can exist. Nitroxides can undergo oxidation to the corresponding oxoammonium cation by various oxidants such as hypervalent haem, $HO_2\cdot$, $CO_3^{-}\cdot$, and $NO_2^{-}\cdot$ radicals (Krishna et al 1992, 1996a, b; Goldstein et al 2006). Thus, in tumours, low levels of oxidative stress may generate these species, which can decrease the nitroxide levels faster than in normal tissue. Oxoammonium cations can be reduced to the nitroxide state by superoxide at diffusion-limited rates or to the hydroxylamine by 2-electron reducing agents (Krishna et al 1996a). Nitroxides can also be reduced to the corresponding hydroxylamines by reductants such as ascorbate, semiquinone radicals and also by intercepting reducing equivalents from the electron transport chain (Swartz 1990). The hydroxylamines can be oxidized to the nitroxides in the presence of hydrogen peroxide and other oxidants such as transition metal complexes (DeGraff et al 1994). In-vitro, nitroxides were found to undergo accelerated conversion to hydroxylamines under hypoxic conditions compared with normoxia (Chen et al 1989). Furthermore, in normoxic cells the conversion was significantly retarded when the thiol levels were depleted or in cells deficient in the enzyme glucose-6-phosphate dehydrogenase (Kuppusamy et al 2002; Samuni et al 2004). The nitroxide/oxoammonium cation pair constitutes an efficient redox couple and mimics the enzymic action of superoxide dismutase (SOD) in a pH-dependent manner (Krishna et al 1996a) and also confers catalase-like action to haem proteins such as myoglobin, cytochrome C, etc. (Krishna et al 1996b). The nitroxide radical, though chemically stable, can participate in radical–radical recombination reactions with a variety of free radicals possessing a wide range of reactivity. The hydroxylamine, on the other hand, can function as a classic antioxidant, such as thiols, ascorbate, etc., by donating the H atom. Its reaction efficiency depends on the species with which it interacts. With highly reactive species such as OH radicals, the hydroxylamine is an efficient scavenger, whereas with species of moderate oxidation potential, hydrogen atom donation by the hydroxylamine proceeds slowly.

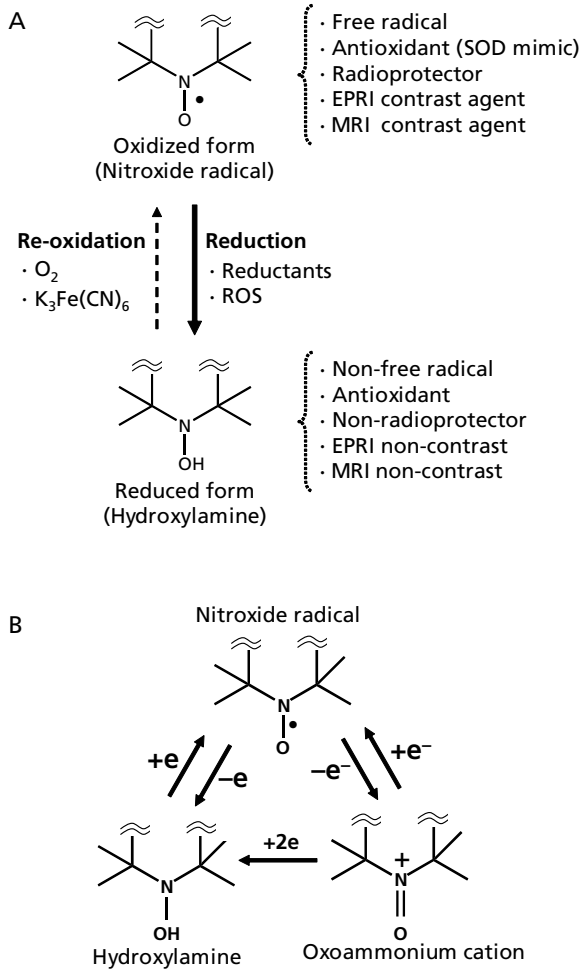

Figure 1 A. Reversible one-electron reduction/oxidation showing the inter-conversion between the oxidized nitroxide (EPRI and MRI contrast) and the corresponding reduced hydroxylamine (EPRI and MRI non-contrast). B. Conversion of nitroxide radical to hydroxylamine or oxoammonium cation in-vivo. Nitroxide compounds are found in-vivo in an equilibrium between the nitroxide radical form, which is detected by EPR, and the reduced form, known as the hydroxylamine, which is not detected. This equilibrium is dependent on the oxygen status and redox status of the tissue milieu. Cellular redox processes convert the compound between the two states, thus the ratio of the two states is determined by the redox activity within the cell.

As mentioned above, nitroxides exert SOD-mimicking activity. SOD is an antioxidant enzyme that detoxifies superoxide it but is too large to cross cell membranes, making it difficult to accumulate it intracellularly by adding exogenous SOD. Unlike SOD, nitroxides can readily cross cell membranes and thus provide intracellular antioxidant availability (Mitchell et al 2000). Nitroxides have been shown to protect against superoxide, hydrogen peroxide, organic peroxides and ionizing radiation (Mitchell et al 2000).

Nitroxides as EPRI contrast agents

Nitroxides have been used as in-vivo EPR spectroscopy/imaging probes to elucidate redox mechanisms in many disease models (Berliner et al 1987, 1998, 2002; Yamada et al 2002; Utsumi & Yamada 2003). Nitroxides were found in-vivo to be in an equilibrium between the nitroxide radical form, which is detected by EPR, and the reduced form, the hydroxylamine, which is not detected by EPR because of its diamagnetic nature (Samuni et al 1990; Swartz 1990). This equilibrium is dependent on the surrounding environment, specifically tissue oxygen and the levels of reducing equivalents of the tissue milieu (Swartz 1990). Cellular redox processes convert the compound between the two states, thus the ratio of the two states is determined by the redox status within the cell (Figure 1B). Since only the oxidized form of the nitroxide can be detected using EPR, signal intensity can be used as a surrogate marker for the relative amounts of the oxidized compound and, therefore, the relative redox activity. In hypoxic cells (which are present in many tumours), the hydroxylamine form is more prevalent, whereas the compound can be oxidized to the radical form in well-oxygenated tissues (Swartz et al 1986b). This property of nitroxides makes them ideal compounds for studying intracellular redox metabolism.

The redox environment (Schafer & Buettner 2001) of the tumour is an important parameter that may determine the response of a tumour to certain chemotherapeutic agents, radiation and bio-reductive hypoxic cell cytotoxins (Griffith 1982; Yu & Brown 1984; Mitchell & Russo 1987; Brown 1993; Stratford et al 1994). A variety of intracellular molecules may contribute to the overall redox status in tissues, including GSH, thioredoxins, NADPH, flavins, ascorbate and others (Schafer & Buettner 2001). Collectively, the reducing species may have an impact on how a particular tissue responds to oxidative stress induced by a particular drug or treatment modality. Therefore, a non-invasive means of determining the redox status of a tissue should be a useful adjunct in clinical oncology.

The bioreduction of nitroxides in RIF-1 tumours implanted in mice was compared with that in normal tissue (Kuppusamy et al 2002; Yamada et al 2002). Pharmacokinetics of nitroxide uptake and clearance from normal and tumour tissues of RIF-1 tumour-bearing mice were measured in-vivo using EPR spectroscopy (Figure 2, 3A). EPR spectra were measured continuously from the tumour on the right leg or normal muscle tissue on the left leg following injection of the nitroxide carbamoyl-PROXYL (3-carbamoyl-2, 2,5,5-tetramethylpyrrolidine-N-oxyl, 3-CP). Using this technology, two-dimensional images of the tumour revealed significant heterogeneity in both nitroxide distribution and rate of reduction (Figure 3 B, C). Nitroxide concentrations in the tumour, as well as normal tissues, decreased linearly with time, suggesting that the clearance pharmacokinetics could be modelled by a pseudo-first-order rate equation. Disappearance of the nitroxide was faster in tumour than in normal muscle tissue (Kuppusamy et al 1998). A series of studies were conducted to determine if the reduction profiles in tumours could be altered by oxygenating the tumour by allowing the tumour-bearing animal to breathe carbogen. Upon oxygenating the tumour, EPRI was conducted as described above and significantly slower nitroxide reduction rates in the tumour were observed (Kuppusamy et al 1998). These data were consistent with the notion that cell/tissue hypoxia is an effective means to reduce nitroxides. The influence of endogenous thiols such as GSH, which is important in maintaining the intracellular redox balance, was also evaluated by using inhibitors of GSH synthesis or agents that bind and deplete GSH (Kuppusamy et al 2002; Yamada et al 2002). When GSH levels were depleted in the tumour by 40–50%, EPRI assessed nitroxide reduction rates in the tumour were markedly slower. Collectively, the EPRI nitroxide reduction studies established, firstly, that the nitroxide is reduced more rapidly in the tumour tissue compared with normal muscle tissue in the tumour-bearing mice and, secondly, that the nitroxide reduction rate constant is decreased when GSH levels are partially depleted or when the tumour oxygen concentration was increased by carbogen breathing. While the EPRI studies were important in establishing 'proof of principle' for redox imaging, the lack of anatomic information from the EPRI and the long imaging times required for 3D imaging precluded its further development.

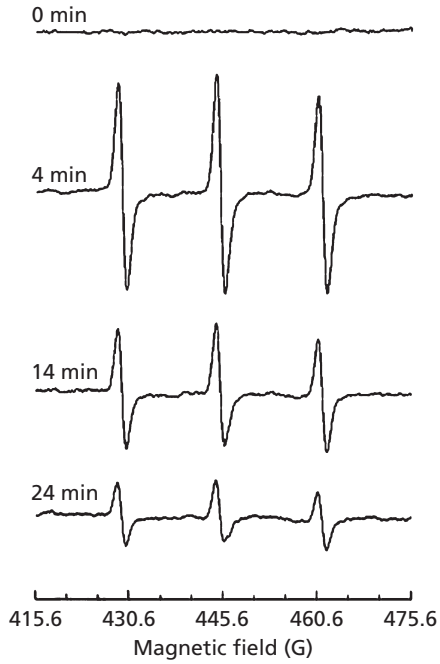

Figure 2 EPR spectra of 3-CP nitroxide in a RIF-1 tumour. A tumour-bearing mouse under anaesthesia was infused intravenously with a saline solution of 3-CP (185 mg kg^{-1}). The uptake and removal of the nitroxide in the tumour tissue was continuously measured in-vivo using an L-band (1.3 GHz) EPR spectrometer. The triplet signal attributable to 3-CP peaked at ~4 min and decayed gradually with a half-life of ~10 min. The triplet, arising because of hyperfine splitting from the 14N nucleus, is characterized with coupling constants 15.78 G and 16.30 G and peak-to-peak width 1.50 G. Measurement parameters: microwave power 8 mW; modulation amplitude, 1.0 G; modulation frequency, 100 kHz; scan time, 15 s. (Adapted with permission from Kuppusamy et al (2002).)

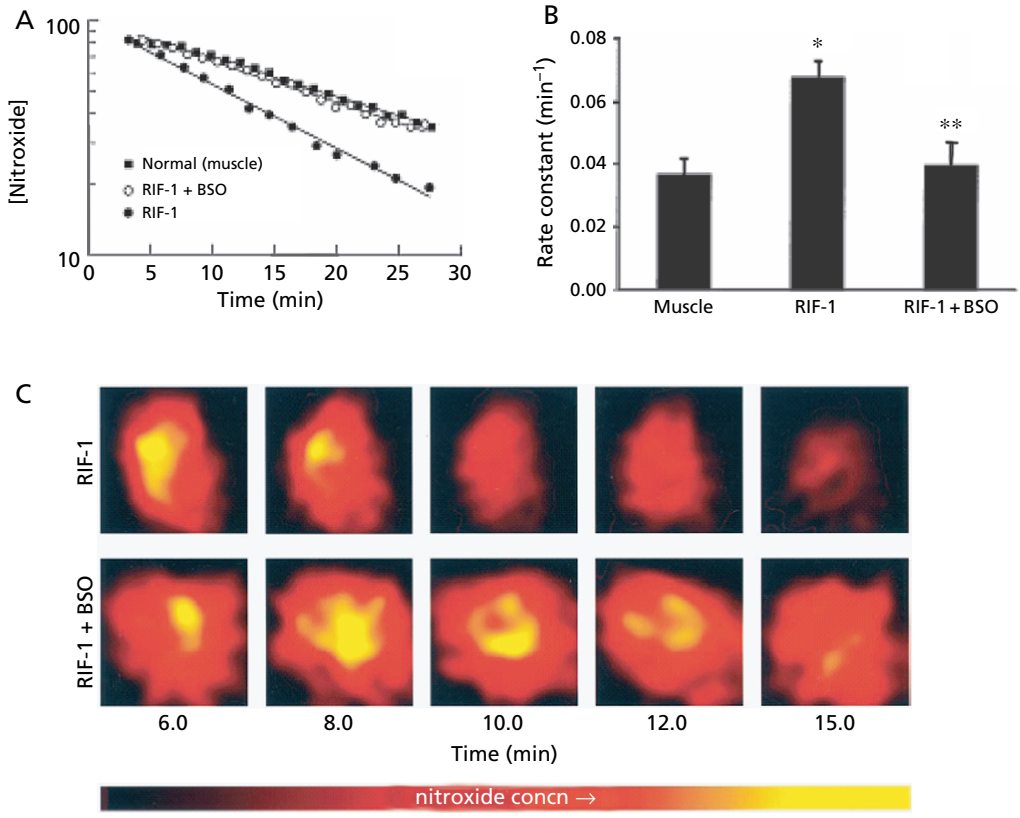

Figure 3 Pharmacokinetics of nitroxide in normal muscle and tumour tissues. Time course of the EPR signal intensity of 3-CP in the normal leg muscle and tumour tissue of RIF-1 tumour-bearing mice, infused intravenously with a saline solution of 3-CP, were obtained by double integration of the spectra. A. The semilog plot shows the clearance of the nitroxide (in arbitrary units) as a function of time in the normal muscle and tumour tissue of untreated tumour-bearing mice and in the tumour tissue of mice treated intraperitoneally with BSO (2.25 mmol kg^{-1}) 6 h before the measurements. The solid lines through the data points are linear fit to the respective data set, which suggests compliance with a pseudo first-order rate law. B. Bar-graph showing the measured pseudo first-order rate constants of nitroxide reduction in the tissues. The data represent mean ± s.e.m. of measurements on 3–5 mice per group. The rate constants were: untreated normal muscle, $0.037 \pm 0.005\ \text{min}^{-1}$; untreated tumour, $0.063 \pm 0.008\ \text{min}^{-1}$, and BSO-treated tumour, $0.052 \pm 0.006\ \text{min}^{-1}$. *$P < 0.05$, vs normal muscle; **$P < 0.05$, vs untreated RIF-1 tissue. C. Spatially resolved clearance of nitroxide in RIF-1 tumour tissue. After tail-vein infusion of 3-CP, a series of two-dimensional images of the nitroxide from tumour (untreated and BSO-treated) were measured using the L-band EPRI method. A few selected images and the corresponding approximate time after infusion are shown. The images represent the mean nitroxide concentration in a two-dimensional projection of the tissue volume ($10 \times 10\ \text{mm}^2$; depth, 5 mm) averaged over 1.5–2.0 min. The image data were acquired using a magnetic field gradient of 15 G cm^{-1} at 16 orientations in the two-dimensional plane. Each image within a series was normalized with respect to the maximum intensity in that series. The nitroxide in the tumour of BSO-treated mouse persisted longer, compared with that in the untreated mouse. (Adapted with permission from Kuppusamy et al (2002).)

Nitroxides as MRI redox-active contrast agents

As mentioned above, EPRI lacks the ability to co-register anatomy with the images of nitroxides' spatial distribution (Kuppusamy et al 1998, 2002; Hyodo et al 2008; Matsumoto et al 2006; Cotrim et al 2007). MRI provides images with useful spatial and temporal resolutions and, with the use of suitable contrast agents, can provide important functional information pertaining to blood flow and tissue perfusion. A number of applications with regard to characterization of disease and assessment of disease response to therapy have emerged using well-established techniques in MRI and suitable choice of contrast media (Silva et al 2000; Barbier et al 2001; Dunn et al 2002; Shapiro et al 2004; Provenzale et al 2006). Conventional contrast agents used for T_1-contrast enhancement in MRI contain paramagnetic entities such as Gd^{3+} and Mn^{2+} complexes. Nitroxide radicals have a single unpaired electron and can provide T_1-contrast similar to gadolinium complexes. Although nitroxides (0.16 ~ 0.18 mM^{-1}s^{-1}) compare unfavourably to Gd^{3+}-containing agents in terms of relaxivity (3.7 mM^{-1}s^{-1}), they are cell permeable and have a larger volume of distribution meaning they can provide useful T_1-contrast enhancement per unit volume (Hyodo et al 2008).

The feasibility of using nitroxides as T_1-contrast agents was examined in the early days of MRI contrast probe development (Brasch 1983; Brasch et al 1983) and before their use as in-vivo EPRI probes (Berliner & Fujii 1985). However, at the time they were found not to be optimal MRI contrast agents (Keana & Pou 1985) because in-vivo the paramagnetic nitroxide radicals were reduced to the undetectable diamagnetic hydroxylamine and they were thus deemed

unstable contrast probes for MRI (Swartz et al 1986a; Keana et al 1987; Chen et al 1989). Because of our experience with nitroxides in EPRI as described above and with the time-efficient image data acquisition strategies standard in current MRI scanners, we re-evaluated nitroxides as functional redox-sensitive probes using MRI. There are many technical challenges using nitroxide contrast agents in MRI. Nitroxide relaxivity is 20 times less than Gd^{3+} complexes. Additionally, since nitroxides can react with reducing species in the body, they easily lose contrast ability. Therefore, fast acquisition sequences and high-field magnets are required. The major advantages of using nitroxides in MRI as opposed to EPRI include the availability of high resolution MRI scanners for both human and small animal studies, multi-slice imaging capability, enhanced spatial and temporal resolution and co-registration of images of tissue redox status with anatomical/functional (water apparent diffusion coefficient, blood flow, blood volume, etc.) information that can be available from MRI. The image enhancement in MRI is dependent on the original T_1 relaxation time of the tissue examined and its variation by free radicals, which is related to the accessibility of the radical to water protons. Therefore, image enhancement in tissue with a given T_1 should depend on the nitroxide concentration (Figure 4). On the other hand, image enhancement is affected by change in spectral shape and height in EPRI in addition to the concentration (Figure 4) (Matsumoto et al 2007). The near-independence of the relaxivity on the nature of nitroxide makes it easy to compare tissue redox status by MRI, whereas in EPRI, the line width and spectral multiplicity determines the image quality in terms of resolution and dynamic range. Continuous measurements of nitroxide levels detect similar decay rates from all three modalities (Figure 5). The similar decay rates obtained from the phantom using MRI and EPRI, which is an accepted method in monitoring nitroxide levels, validate the use of MRI for such studies. Multi-slice images were obtained in 20 s using the SPGR method (Figure 5C). This scanning allows fast pharmacokinetic imaging, besides providing detailed anatomical structure unlike in EPRI. In addition to anatomical structure, dynamic information, such as blood flow, blood volume and water diffusion coefficients, etc., can be monitored by MRI and compared with redox images.

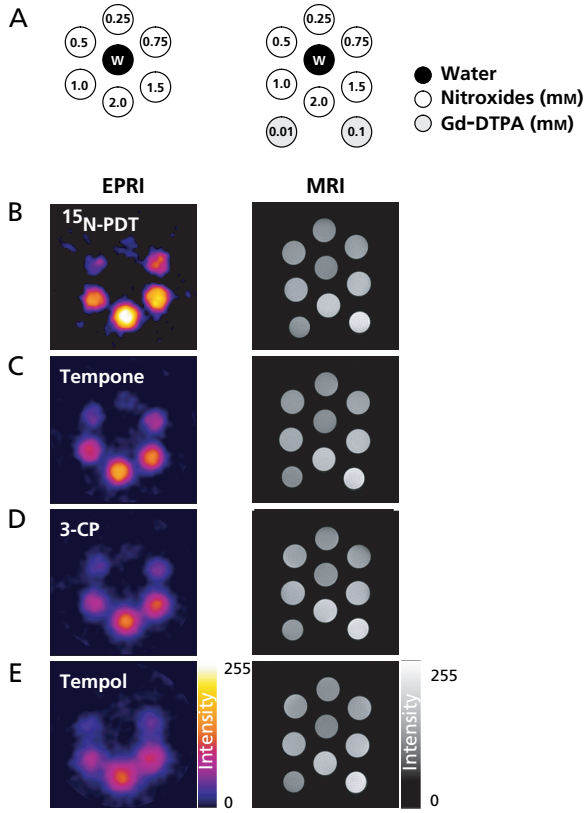

Figure 4 The phantom images of four nitroxides obtained by EPRI and MRI. A. Schematics of the phantom. Additionally two tubes of 0.01 and 0.1 mM Gd-DTPA solution were added during MRI measurement. B–E. The EPRI (left column) and MR (right column) intensity images of ^{15}N-PDT (B), Tempone (C), 3-CP (D) and Tempol (E) were described. EPRI conditions were as follows; 18 projections were obtained every 1 min. FOV was 3.2 × 3.2 cm. Microwave frequency was 300 MHz, microwave power 2.5 mW, field modulation frequency was 13.5 kHz, time constant 0.01 s, gradient was 4.7 G cm^{-1} and sweep width was 50 Gauss. MRI: SPGE sequence (TR = 75 ms, TE = 3 ms, Flip angle = 45°, NEX = 2) was employed to observe T_1 effect. Pixel resolution was 256 × 256. FOV was 3.2 × 3.2 cm. All measurements were performed at room temperature (25 ± 2°C). (Adapted with permission from Hyodo et al (2008).)

In-vivo redox MRI of tumour redox status

Nitroxide reduction as assessed by MRI or EPRI was first validated in phantoms containing the nitroxide with a reducing agent (Matsumoto et al 2006). Both EPRI and MRI experiments showed similar nitroxide reduction rates, suggesting that the T_1 contrast capability of nitroxides was amenable to monitoring changes in image intensity using MRI. Next, differences in nitroxide 3-CP metabolism in tumour and normal tissues were evaluated in tumour-bearing mice as shown in Figure 6A. As can be seen in Figure 6B, the MRI signal intensity increased in both the normal the and tumour-bearing leg following 3-CP administration and reached a maximum. However, the subsequent decrease in signal intensity in the tumour region was faster than that seen in normal tissue (Figure 6B). The signal reduction rate in the regions of interest (ROI) chosen in the normal leg was observed to be approximately 60% that of the reduction rate in the ROI in the tumour (Figure 6C). The rate of change of intensity in each pixel was computed and a parametric image showed that overall tumour reduction was elevated as compared with normal tissue (Figure 6D). The significant enhancement in image intensity induced by 3-CP administration and the superior temporal and spatial resolution of MRI suggest that it is advantageous to monitor the pharmacokinetic distribution of nitroxides using T_1-weighted MRI instead of EPRI.

To confirm that the decrease in nitroxide image intensity as shown in Figure 6B–D was due to reduction instead of clearance, an independent study was conducted (Hyodo et al 2006). Three different nitroxides were used of which two were cell-permeable nitroxides (Tempol, 3-CP) and one a cell-impermeable nitroxide (3-carboxy-2,2,5,5,5-tetramethylpyrrolidine-l-oxyl (CxP)). Reduction of these nitroxides was examined in normal muscle, tumour, and artery area simultaneously using

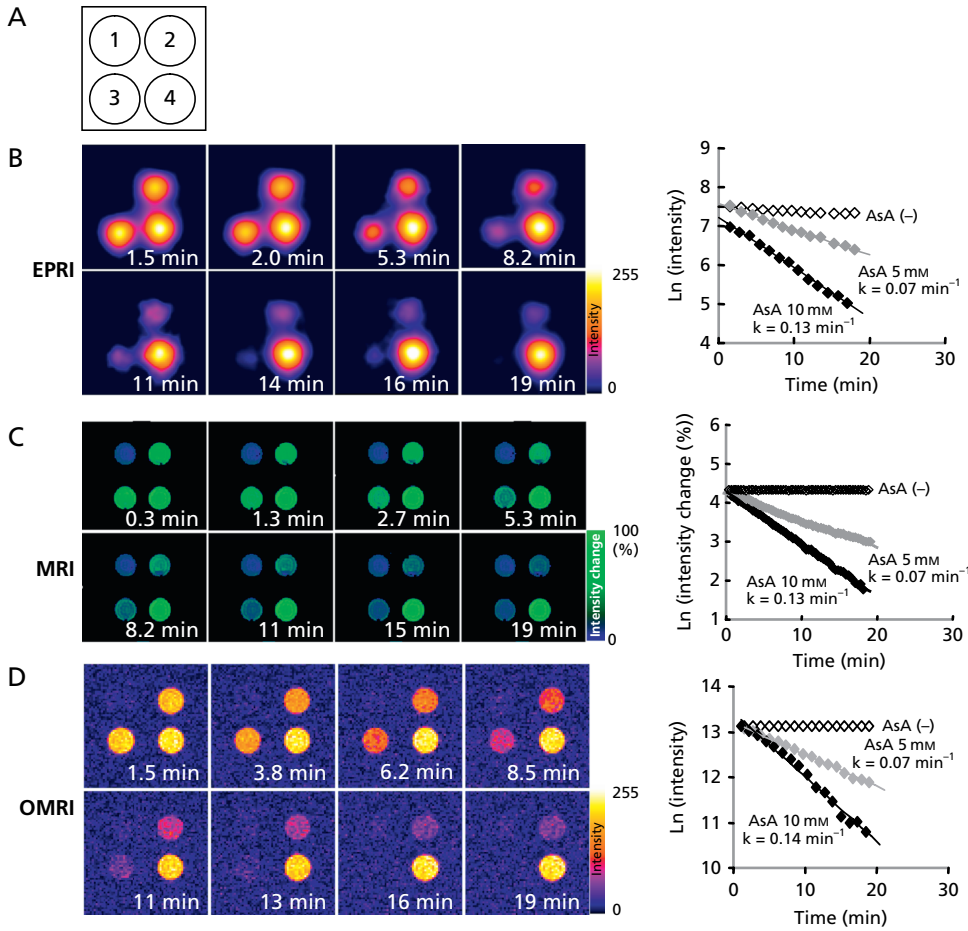

Figure 5 Comparison of image intensity decay among three modalities. A. Schematic of the phantoms: tube 1, PBS; tube 2, 2 mM 3-CP and 5 mM ascorbic acid (AsA); tube 3, 2 mM 3-CP and 10 mM AsA; tube 4, 2 mM 3-CP. B–D. Time course images and decay slopes of EPRI (B), MRI (C) and Overhauser MRI (OMRI) (D) were obtained. After addition of AsA/PBS solution, the EPRI or OMRI measurements were started immediately and continuously measured up to 20 min. In the case of MRI, AsA/PBS was added using PE-10 tube 2 min after scanning was started. Therefore, time zero in the MRI experiment represents the time at addition of AsA solution. The experiments were repeated three or four times using with freshly prepared solutions. Semi-logarithmic plots of the time course of MRI signal change in the region of interest (ROI: 10 ×10 pixels) were used for decay rate calculation using imageJ software. Decay rate constants were obtained from the slope of linear portion of the decay curves. (Adapted with permission from Hyodo et al (2008).)

MRI (SPGR to acquire 6 slices every 20 s). In parallel groups of animals injected with the nitroxides, tissue samples were taken over the same time period for ex-vivo determination of total nitroxide concentration (oxidized plus reduced) by EPR spectroscopy. MRI-assessed nitroxide reduction rates and total nitroxide present in the tissues are shown in Figure 7 and Table 1 for normal muscle, tumor, and blood. The two cell-permeable nitroxides, Tempol and 3-CP, exhibited distinct differences in the reduction rates of image intensity between normal and tumour tissue. In the case of Tempol, the decay rate in the tumour was ~3.5 times that observed in the normal tissue. For 3-CP, the decay rate in the tumour was ~2 times higher than in the normal leg. The total levels of Tempol and 3-CP (nitroxide + hydroxylamine) as measured by EPR spectroscopy over the same time period in tumour and muscle homogenates was relatively constant, suggesting that the decrease in nitroxide image intensity in MRI was a result of intracellular reduction of the nitroxide. In the case of the cell-impermeable nitroxide 3CxP, no significant differences in MRI signal decay rates between tumour and muscle tissue were detected, and the MRI decay rates essentially parallelled the nitroxide tissue levels as examined by EPR. Similar findings were obtained in blood, suggesting that the reduction of Tempol and 3-CP in the blood is a result of global intracellular reduction and not clearance. Since 3CxP, is cell impermeable, it was not reduced as shown by both MRI assessment and total nitroxide present in the blood. Nitroxide reduction rates for tissues just described and a few other tissues are shown in Table 1. These studies firmly establish the use of cell-permeable nitroxides coupled with MRI to non-invasively examine differences in the redox status of tissues. While particular emphasis has been placed on differences in the redox status in tumours compared with selected normal tissues, the technique possesses the potential to have broad applications to the study of other disease states, inflammatory processes and other circumstances in which oxidative stress is implicated.

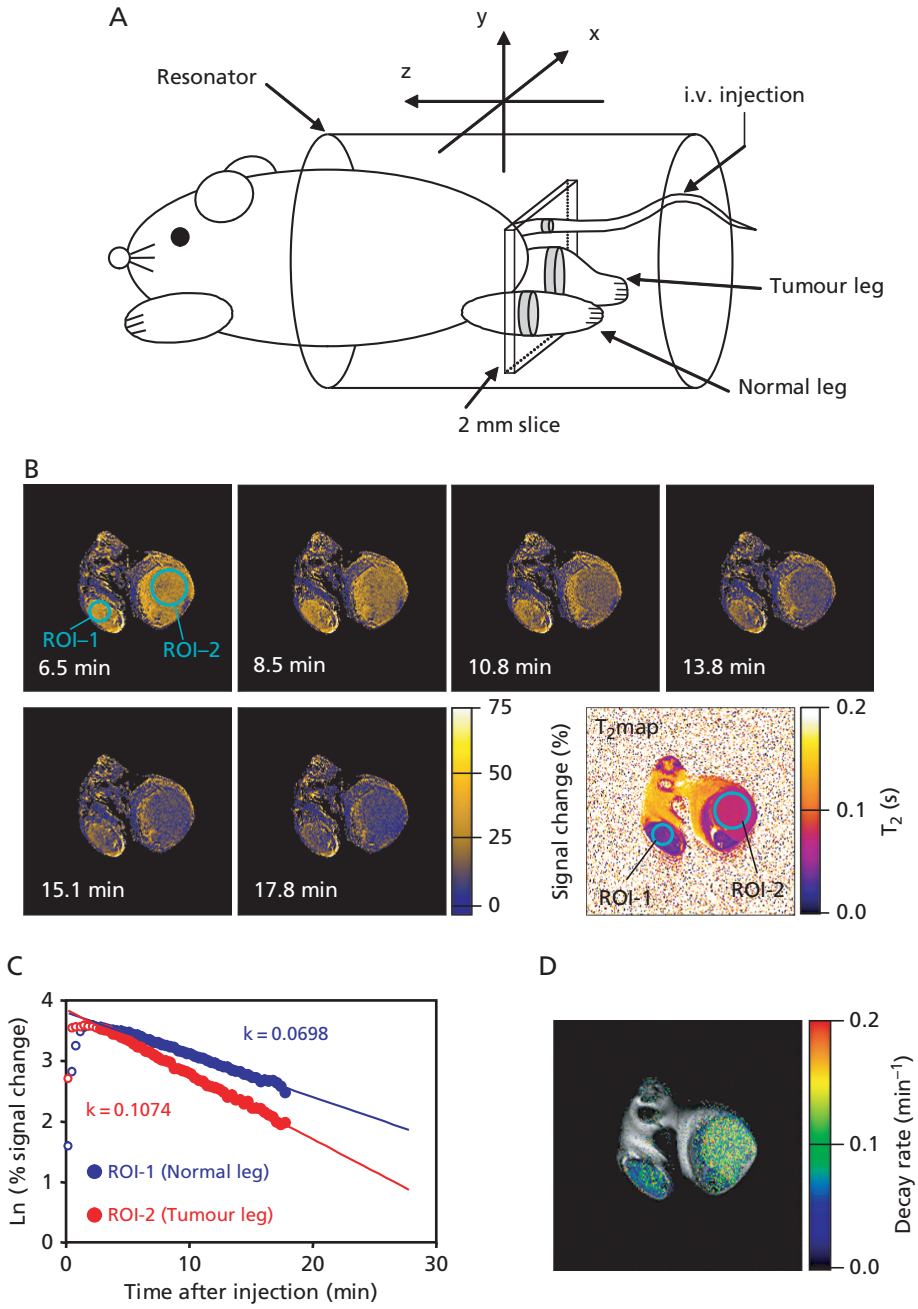

Figure 6 A. Experimental arrangement of the mouse in the MRI resonator and the slice selected to monitor the nitroxide levels used to examine the differences in nitroxide metabolism in tumor and normal tissue. B. Sequence of T_1-weighted MR images as a function of time after intravenous administration of 3-CP. Signal intensity in normal (ROI-1) and tumor leg (ROI-2) increased after 3CP administration and reached a maximum at 8.5 min. The nitroxide signal decreased thereafter faster in tumour region (ROI-1) than in normal tissue (ROI-2). C. The rate of intensity change in each pixel was computed for each ROI and plotted as a function of time. The rate of intensity change in the normal leg was observed to be ~60% compared with that in tumour. D. Parametric image redisplayed shows that tumour reduction globally is elevated compared with the normal tissue. (Adapted with permission from Matsumoto et al (2006).)

Assessment of selective radioprotection of salivary glands by redox MRI

The ability to selectively protect normal tissues in cancer patients receiving radiation treatment would be most advantageous. If selective protection of normal tissues were possible, higher radiation doses could be delivered to the tumour accompanied by higher local control rates. The key, however, is selective normal tissue protection because if a systemic radioprotector also protects the tumour, no advantage would be realized. Amifostine, an FDA-approved

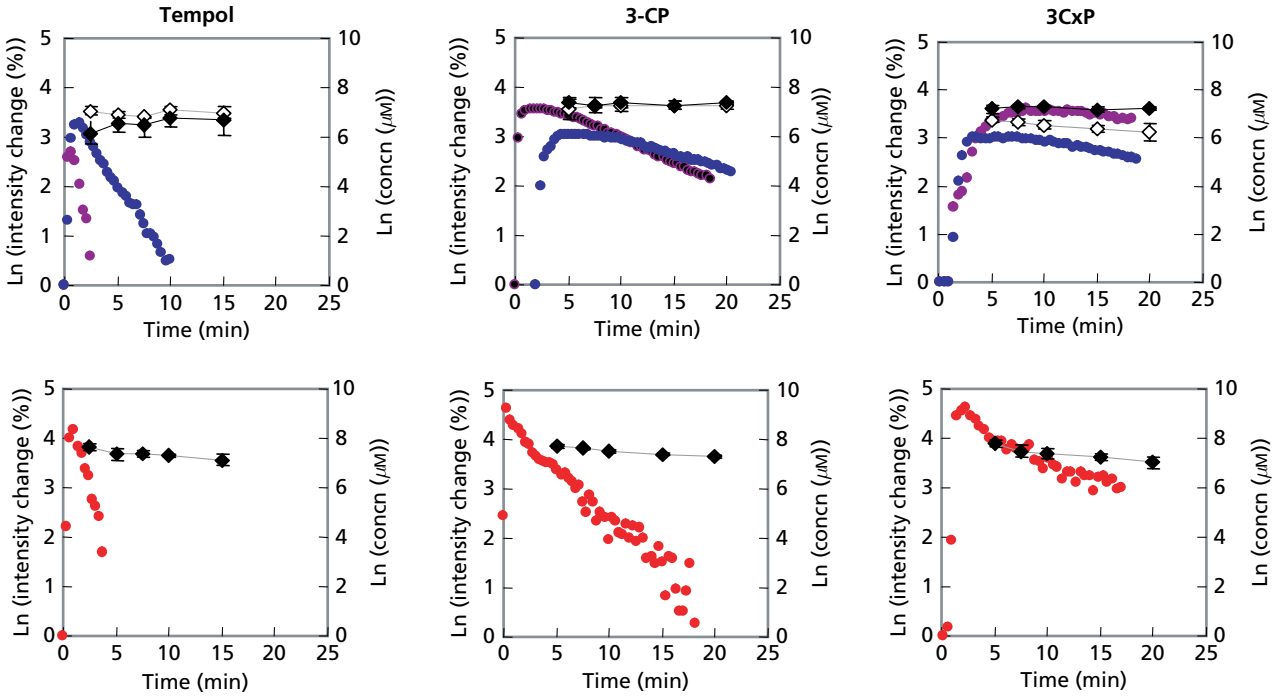

Figure 7 The pharmacokinetics of oxidized form and total (oxidized and reduced form) nitroxide contrast agents in normal leg muscle, tumour and blood. The pharmacokinetics of oxidized form of Tempol (A), 3-CP(B) and 3CxP (C) in normal tissue (blue), tumour tissue (purple) and artery (red) were obtained by SPGR MRI. The total nitroxide contrast agent concentration of Tempol (A), 3-CP (B) and 3CxP (C) in normal tissue (upper figure, gray), tumour tissue (upper figure, black) and blood (lower figure. black) was measured ex-vivo by x-band EPR spectroscopy using 10 mM ferricyanide/PBS solution (final concentration was 2 mM). (Adapted with permission from Hyodo et al (2006).)

Table 1 Decay rate of nitroxide contrast agents in various tissues

Tissue	Decay rate (min^{-1})		
	Tempol	3-CP	3CxP
Normal leg	0.32 ± 0.03	0.056 ± 0.013	0.029 ± 0.014
Tumour leg	1.1 ± 0.2**	0.107 ± 0.020*	0.020 ± 0.014
Blood	1.0 ± 0.2	0.364 ± 0.008	0.4 ± 0.2
Left kidney	1.5 ± 0.2	0.30 ± 0.05	0.046 ± 0.006
Right kidney	1.2 ± 0.3	0.29 ± 0.04	0.050 ± 0.005
Salivary gland	0.79 ± 0.3	ND	ND

Values are indicated as means ± s.d. The three mice after each nitroxide injection (total 9 mice) were measured and obtained serial images (total 360 images) of six slices of each mouse during 20 min. *$P < 0.05$, **$P < 0.01$, muscle vs tumour. T_1-weighted images (6 slices and 60 continuous imaging: total 360 images) were acquired over 20 min, using SPGR. A solution of nitroxide contrast agents in PBS (1.5 μmol/g b.w.) was injected via tail-vein cannulation, 2.0 min after starting scan. The conditions of MRI were follows; TR = 75 ms, TE = 3 ms, FA = 45°, N_{EX} = 2, scan time = 20 s. Image resolution = 256 × 256, FOV was 3.2 × 3.2 cm, slice thickness was 2.0 mm. Number of slices was 2. (Adapted with permission from Hyodo et al (2006) and Cotrim et al (2007).)

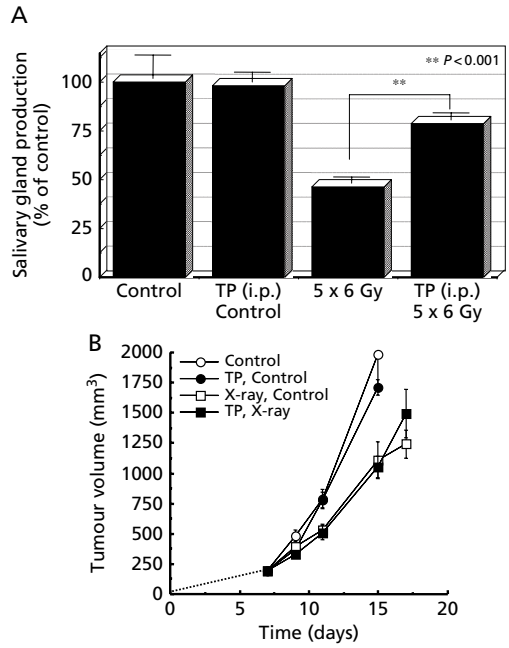

Figure 8 A. Salivary gland production for fractionated radiation treatment with and without Tempol administration. B. Radiation tumour (SCCVII) regrowth study for local fractionated radiation treatment with and without Tempol administration. Tumours received 5 daily fractions (Monday–Friday) of 3 Gy (SCC VII) or 2 Gy (HT-29). Arrows on each plot indicate the days when radiation treatment was administered. (Adapted with permission from Cotrim et al (2007).)

radioprotector for xerostomia (Koukourakis 2002; Scully et al 2006), remains controversial with respect to its ability to protect tumour as well as normal tissues (Yuhas 1983; Brizel & Overgaard 2003).

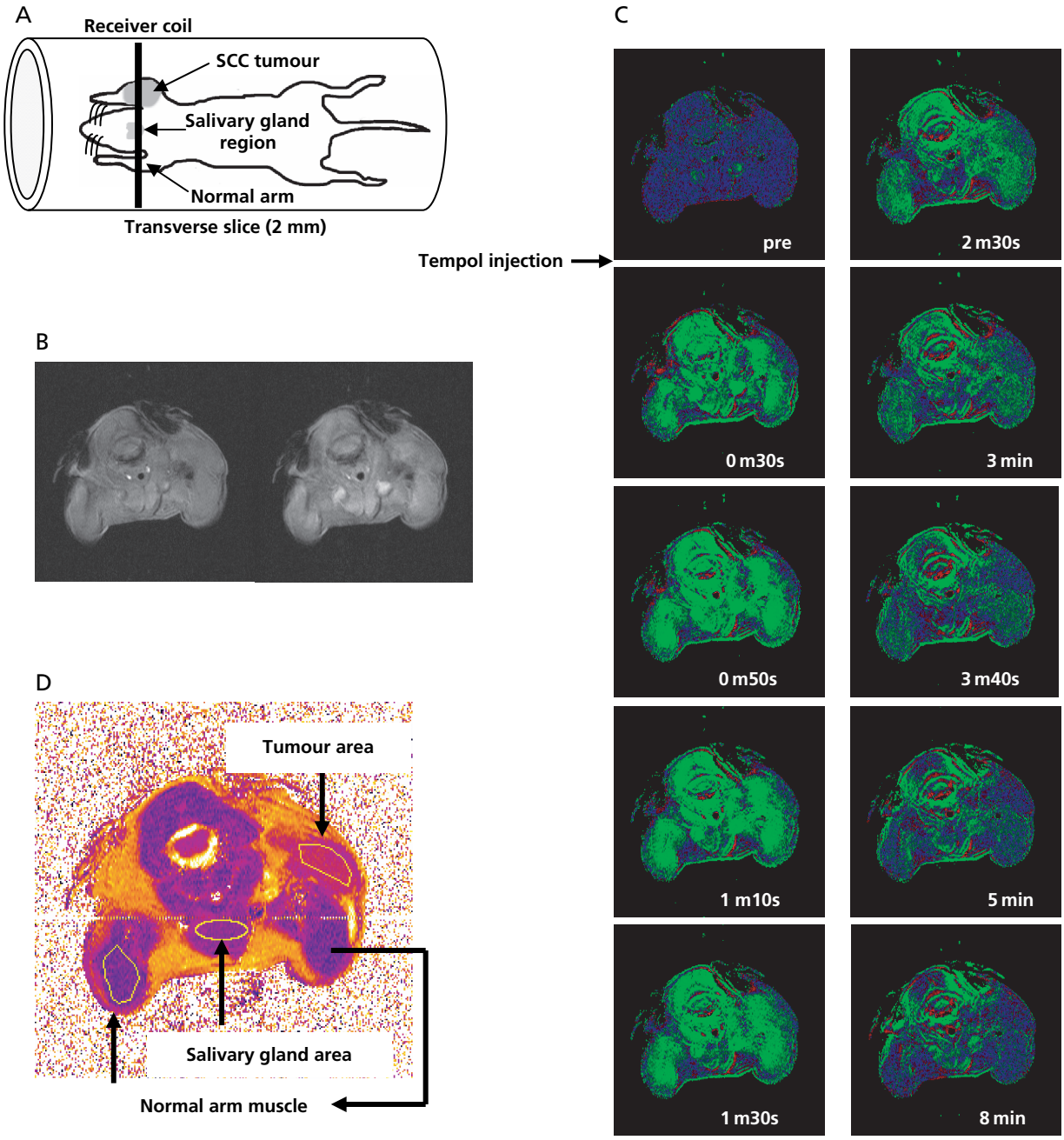

Figure 9 A. Schematic of the placement of the mouse in the resonator and the slice selected for MRI experiments. A transverse slice (2 mm) covering the normal muscle tissue (Greenlee et al 2001), salivary gland and the tumour in the contralateral leg was chosen to monitor nitroxide levels as a function of time. B. T_2-weighted images of adjacent slices before injecting Tempol to ensure that the target tissues were in the field of view. C. T_1-weighted images of the selected region before injection of Tempol and as a function of time after intravenous Tempol injection. D. T_2 map of the slice and the regions of interest chosen in the normal leg, salivary gland and tumour to monitor Tempol decay rates. (Adapted with permission from Cotrim et al (2007).)

In-vitro studies have clearly shown that nitroxide (oxidized form) is radioprotective, whereas, the hydroxylamine (reduced form) does not provide protection (Mitchell et al 1991, 2003; Krishna et al 1998). Likewise, we have previously shown that Tempol protects against whole-body radiation-induced lethality, with a dose-modifying factor of 1.4 (Hahn et al 1992). Tempol, when given at the same dose and timing (275 mg kg^{-1}, 10 min before radiation) as was used in whole body radiation study, did not protect against local single radiation doses delivered to RIF tumours based on TCD50 comparisons (Hahn et al 1997). It was demonstrated in this study that Tempol was reduced to the non-radioprotective

hydroxylamine faster in the tumour than in bone marrow (Hahn et al 1992). Thus, at the time of radiation (10 min post-injection of Tempol), a higher concentration of Tempol (radioprotective) was present in the normal tissue (bone marrow) than in the tumour when the Tempol levels were measured in the respective tissues ex-vivo using EPR spectroscopy.

More recent studies have demonstrated that Tempol protects against radiation-induced salivary gland damage, but not against radiation-induced tumour regrowth delay (Figure 8) (Cotrim et al 2007). Five daily fractions of 6 Gy were delivered to only the animal's head. Tempol was injected (275 mg kg^{-1} i.p.) 10 min before each radiation fraction. As can be seen in Figure 8A, 5×6 Gy resulted in a reduction of saliva production ~54%. Five daily treatments of Tempol (i.p.) alone exhibited no toxicity and had no effect on salivary gland function (Figure 8A); however, Tempol (i.p.) provided significant protection ($P < 0.001$) against radiation-induced salivary gland damage in replicate experiments. Figure 8B shows that administering Tempol at the same dose and timing as used in Figure 8A had no influence on radiation-induced tumour regrowth delay. MR assessment of tissue levels of Tempol for each tissue (normal leg muscle, salivary gland region and tumour) was also determined (Figure 9A). Transverse MR images were acquired to ensure that the target tissues were within the 2-mm slice selected for imaging (Figure 9B). Dynamic T_1-weighted MR scans were then acquired before and after Tempol injection (Figure 9C). The green areas showed enhancement in MR intensity by Tempol, which quickly appeared at 30 s, peaked at ~1 min, and then gradually disappeared 8 min after injection. To establish the rate of disappearance (reduction) of Tempol in various tissues, selected ROI were outlined (Figure 9D) and MR intensity changes by Tempol in normal leg muscle, salivary gland region and tumour were plotted as a function of time after injection (Figure 10A). The decay in Tempol-mediated MR intensity was similar for normal leg muscle and the salivary gland region; however, the decay rate was significantly faster in the tumour region (Figure 10B). These results suggest that Tempol provided salivary gland radioprotection and did not protect tumour, consistent with the hypothesis by the redox MRI results that differential radioprotection resides in faster reduction to the non-radioprotective hydroxylamine in tumour compared with normal tissues (Cotrim et al 2007).

This study provides the feasibility of evaluating Tempol as a radioprotector in clinical trials for patients with head and neck cancer being treated with radiation and utility of redox MRI. Coupling MRI with such a trial would permit a novel dimension that could provide extremely important information with respect to the timing of Tempol administration and radiation treatment. For example, before radiation treatment, a pilot Tempol/MRI study could be conducted to determine Tempol reduction rates of tumour and normal tissues encompassed in the proposed treatment field. Based on these reduction rates, the optimal timing of Tempol administration with respect to radiation treatment to provide selective radioprotection to normal tissues could be determined. The unique aspect of such an approach is made possible because the therapeutic agent in this case (Tempol) can be visualized by MRI. There are few therapeutic agents used in cancer management (excluding radiolabelled agents) that can be followed by noninvasive imaging. Before such an approach could be considered for clinical trials, more research will be required, such as whether Tempol reduction rates in tissues change during fractionated radiation treatment.

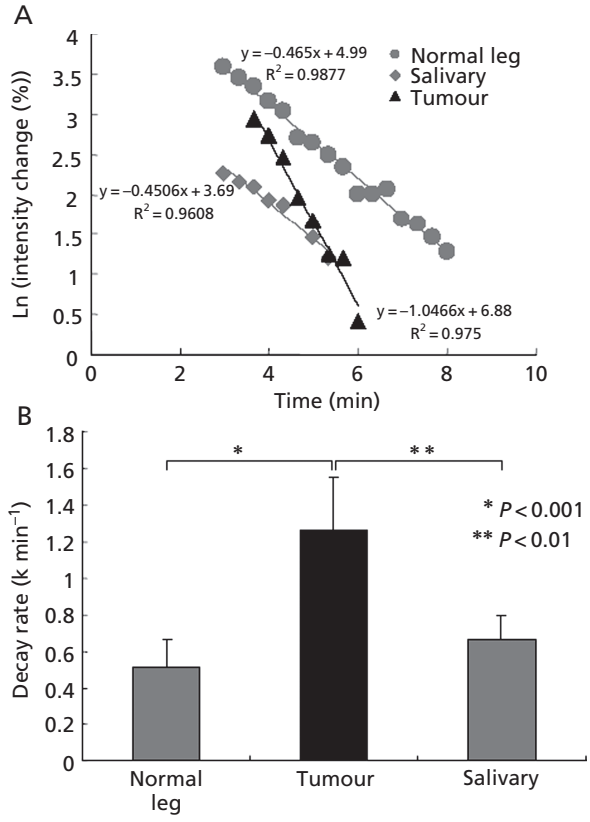

Figure 10 A. Representative Tempol decay rates after intravenous injection in a mouse for the selected regions of interest shown in Figure 5D. B. Summary of decay rates from the three regions of interest in normal muscle, salivary gland and tumour. (Adapted with permission from Cotrim et al (2007).)

Conclusions

Monitoring profiles of reduction/oxidation of nitroxide/hydroxylamines may actually serve as a viable approach to assess the global redox status in tissue using EPRI or MRI. The pharmacokinetics of the nitroxide can be obtained using either EPRI or MRI. Although EPRI can detect nitroxide free radicals directly and obtain images of nitroxide free radical distribution as well as redox maps, the poor image resolution and lack of anatomical detail limit its use in the clinical setting presently. On the other hand, the T_1-weighted MRI serves as an indirect detection modality of nitroxide contrast agents. The T_1-weighted spoiled gradient echo-based dynamic MRI can give appropriate tumour redox status information with useful anatomical resolution. Functional nitroxide redox MRI could be used in the clinical setting to monitor redox changes in tumour and normal tissue in patients undergoing radiotherapy and other types of cancer treatment. Likewise, its potential applications in various disease states resulting from oxidative stress and inflammation remain to be explored.

References

Barbier, E. L., Lamalle, L., Decorps, M. (2001) Methodology of brain perfusion imaging. *J. Magn. Reson. Imaging* **13**: 496–520

Berliner, J. L., Fujii, H. (1985) Magnetic resonance imaging of biological specimens by electron paramagnetic resonance of nitroxide spin labels. *Science* **227**: 517–519

Berliner, L. J., Fujii, H., Wan, X. M., Lukiewicz, S. J. (1987) Feasibility study of imaging a living murine tumor by electron paramagnetic resonance. *Magn. Reson. Med*. **4**: 380–384

Brasch, R. C. (1983) Work in progress: methods of contrast enhancement for NMR imaging and potential applications. A subject review. *Radiology* **147**: 781–788

Brasch, R. C., London, D. A., Wesbey, G. E., Tozer, T. N., Nitecki, D. E., Williams, R. D., Doemeny, J., Tuck, L. D., Lallemand, D. P. (1983) Work in progress: nuclear magnetic resonance study of a paramagnetic nitroxide contrast agent for enhancement of renal structures in experimental animals. *Radiology* **147**: 773–779

Brizel, D. M., Overgaard, J. (2003) Does amifostine have a role in chemoradiation treatment? *Lancet Oncol*. **4**: 378–381

Brown, J. M. (1993) SR 4233 (tirapazamine): a new anticancer drug exploiting hypoxia in solid tumours. *Br. J. Cancer* **67**: 1163–1170

Chen, K., Glockner, J. F., Morse, P. D., Swartz, H. M. (1989) Effects of oxygen on the metabolism of nitroxide spin labels in cells. *Biochemistry* **28**: 2496–2501

Cotrim, A. P., Hyodo, F., Matsumoto, K., Sowers, A. L., Cook, J. A., Baum, B. J., Krishna, M. C., Mitchell, J. B. (2007) Differential radiation protection of salivary glands versus tumor by Tempol with accompanying tissue assessment of Tempol by magnetic resonance imaging. *Clin. Cancer Res*. **13**: 4928–4933

DeGraff, W., Hahn, S. M., Mitchell, J. B., Krishna, M. C. (1994) Free radical modes of cytotoxicity of adriamycin and streptonigrin. *Biochem. Pharmacol*. **48**: 1427–1435

Dunn, J. F., O'Hara, J. A., Zaim-Wadghiri, Y., Lei, H., Meyerand, M. E., Grinberg, O. Y., Hou, H., Hoopes, P. J., Demidenko, E., Swartz, H. M. (2002) Changes in oxygenation of intracranial tumors with carbogen: a BOLD MRI and EPR oximetry study. *J. Magn. Reson. Imaging* **16**: 511–521

Goldstein, S., Samuni, A., Hideg, K., Merenyi, G. (2006) Structure-activity relationship of cyclic nitroxides as SOD mimics and scavengers of nitrogen dioxide and carbonate radicals. *J. Phys. Chem. A* **110**: 3679–3685

Greenlee, R. T., Hill-Harmon, M. B., Murray, T., Thun, M. (2001) Cancer statistics, 2001. *CA Cancer J. Clin*. **51**: 15–36

Griffith, O. W. (1982) Mechanism of action, metabolism, and toxicity of buthionine sulfoximine and its higher homologs, potent inhibitors of glutathione synthesis. *J. Biol. Chem*. **257**: 13704–13712

Hahn, S. M., Tochner, Z., Krishna, C. M., Glass, J., Wilson, L., Samuni, A., Sprague, M., Venzon, D., Glatstein, E., Mitchell, J. B., Russo, A. (1992) Tempol, a stable free radical, is a novel murine radiation protector. *Cancer Res*. **52**: 1750–1753

Hahn, S. M., Sullivan, F. J., DeLuca, A. M., Krishna, C. M., Wersto, N., Venzon, D., Russo, A., Mitchell, J. B. (1997) Evaluation of tempol radioprotection in a murine tumor model. *Free Radic. Biol. Med*. **22**: 1211–1216

Halliwell, B., Gutteridge, J. M. C. (1999) *Free radicals in biology and medicine*. Oxford University Press, London

Herholz, K., Coope, D., Jackson, A. (2007) Metabolic and molecular imaging in neuro-oncology. *Lancet Neurol*. **6**: 711–724

Hoh, C. K. (2007) Clinical use of FDG PET. *Nucl. Med. Biol*. **34**: 737–742

Huzjan, R., Sala, E., Hricak, H. (2005) Magnetic resonance imaging and magnetic resonance spectroscopic imaging of prostate cancer. *Nat. Clin. Pract. Urol*. **2**: 434–442

Hyodo, F., Matsumoto, K., Matsumoto, A., Mitchell, J. B., Krishna, M. C. (2006) Probing the intracellular redox status of tumors with magnetic resonance imaging and redox-sensitive contrast agents. *Cancer Res*. **66**: 9921–9928

Hyodo, F., Murugesan, R., Matsumoto, K. I., Hyodo, E., Subramanian, S., Mitchell, J. B., Krishna, M. C. (2008) Monitoring redox-sensitive paramagnetic contrast agent by EPRI, OMRI and MRI. *J. Magn. Reson*. **190**: 105–112

Keana, J. F., Pou, S. (1985) Nitroxide-doped liposomes containing entrapped oxidant: an approach to the "reduction problem" of nitroxides as MRI contrast agents. *Physiol. Chem. Phys. Med. NMR* **17**: 235–240

Keana, J. F., Pou, S., Rosen, G. M. (1987) Nitroxides as potential contrast enhancing agents for MRI application: influence of structure on the rate of reduction by rat hepatocytes, whole liver homogenate, subcellular fractions, and ascorbate. *Magn. Reson. Med*. **5**: 525–536

Koo, V., Hamilton, P. W., Williamson, K. (2006) Non-invasive in vivo imaging in small animal research. *Cell Oncol*. **28**: 127–139

Koukourakis, M. I. (2002) Amifostine in clinical oncology: current use and future applications. *Anticancer Drugs* **13**: 181–209

Krishna, M. C., Grahame, D. A., Samuni, A., Mitchell, J. B., Russo, A. (1992) Oxoammonium cation intermediate in the nitroxide-catalyzed dismutation of superoxide. *Proc. Natl Acad. Sci. USA* **89**: 5537–5541

Krishna, M. C., Russo, A., Mitchell, J. B., Goldstein, S., Dafni, H., Samuni, A. (1996a) Do nitroxide antioxidants act as scavengers of $O2^{\cdot-}$ or as SOD mimics? *J. Biol. Chem*. **271**: 26026–26031

Krishna, M. C., Samuni, A., Taira, J., Goldstein, S., Mitchell, J. B., Russo, A. (1996b) Stimulation by nitroxides of catalase-like activity of hemeproteins. Kinetics and mechanism. *J. Biol. Chem*. **271**: 26018–26025

Krishna, M. C., DeGraff, W., Hankovszky, O. H., Sar, C. P., Kalai, T., Jeko, J., Russo, A., Mitchell, J. B., Hideg, K. (1998) Studies of structure-activity relationship of nitroxide free radicals and their precursors as modifiers against oxidative damage. *J. Med. Chem*. **41**: 3477–3492

Kuppusamy, P., Chzhan, M., Vij, K., Shteynbuk, M., Lefer, D. J., Giannella, E., Zweier, J. L. (1994) Three-dimensional spectral-spatial EPR imaging of free radicals in the heart: a technique for imaging tissue metabolism and oxygenation. *Proc. Natl Acad. Sci. USA* **91**: 3388–3392

Kuppusamy, P., Afeworki, M., Shankar, R. A., Coffin, D., Krishna, M. C., Hahn, S. M., Mitchell, J. B., Zweier, J. L. (1998) In vivo electron paramagnetic resonance imaging of tumor heterogeneity and oxygenation in a murine model. *Cancer Res*. **58**: 1562–1568

Kuppusamy, P., Li, H., Ilangovan, G., Cardounel, A. J., Zweier, J. L., Yamada, K., Krishna, M. C., Mitchell, J. B. (2002) Noninvasive imaging of tumor redox status and its modification by tissue glutathione levels. *Cancer Res*. **62**: 307–312

Liu, K. J., Bacic, G., Hoopes, P. J., Jiang, J., Du, H., Ou, L. C., Dunn, J. F., Swartz, H. M. (1995) Assessment of cerebral pO_2 by EPR oximetry in rodents: effects of anesthesia, ischemia, and breathing gas. *Brain Res*. **685**: 91–98

Margolis, D. J., Hoffman, J. M., Herfkens, R. J., Jeffrey, R. B., Quon, A., Gambhir, S. S. (2007) Molecular imaging techniques in body imaging. *Radiology* **245**: 333–356

Matsumoto, K., Hyodo, F., Matsumoto, A., Koretsky, A. P., Sowers, A. L., Mitchell, J. B., Krishna, M. C. (2006) High-resolution mapping of tumor redox status by magnetic resonance imaging using nitroxides as redox-sensitive contrast agents. *Clin. Cancer Res*. **12**: 2455–2462

Matsumoto, K., Narazaki, M., Ikehira, H., Anzai, K., Ikota, N. (2007) Comparisons of EPR imaging and T1-weighted MRI for efficient imaging of nitroxyl contrast agents. *J. Magn. Reson*. **187**: 155–162

Mitchell, J. B., Russo, A. (1987) The role of glutathione in radiation and drug induced cytotoxicity. *Br. J. Cancer Suppl*. **8**: 96–104

Mitchell, J. B., DeGraff, W., Kaufman, D., Krishna, M. C., Samuni, A., Finkelstein, E., Ahn, M. S., Hahn, S. M., Gamson, J., Russo, A. (1991) Inhibition of oxygen-dependent radiation-induced damage by the nitroxide superoxide dismutase mimic, tempol. *Arch. Biochem. Biophys*. **289**: 62–70

Mitchell, J. B., Russo, A., Kuppusamy, P., Krishna, M. C. (2000) Radiation, radicals, and images. *Ann. NY Acad. Sci*. **899**: 28–43

Mitchell, J. B., Xavier, S., DeLuca, A. M., Sowers, A. L., Cook, J. A., Krishna, M. C., Hahn, S. M., Russo, A. (2003) A low molecular weight antioxidant decreases weight and lowers tumor incidence. *Free Radic. Biol. Med*. **34**: 93–102

Provenzale, J. M., Mukundan, S., Barboriak, D. P. (2006) Diffusion-weighted and perfusion MR imaging for brain tumor characterization and assessment of treatment response. *Radiology* **239**: 632–649

Samuni, A., Krishna, C. M., Mitchell, J. B., Collins, C. R., Russo, A. (1990) Superoxide reaction with nitroxides. *Free Radic. Res. Commun*. **9**: 241–249

Samuni, Y., Gamson, J., Samuni, A., Yamada, K., Russo, A., Krishna, M. C., Mitchell, J. B. (2004) Factors influencing nitroxide reduction and cytotoxicity in vitro. *Antioxid. Redox Signal*. **6**: 587–595

Schafer, F. Q., Buettner, G. R. (2001) Redox environment of the cell as viewed through the redox state of the glutathione disulfide/glutathione couple. *Free Radic. Biol. Med*. **30**: 1191–1212

Scully, C., Sonis, S., Diz, P. D. (2006) Oral mucositis. *Oral Dis*. **12**: 229–241

Shapiro, E. M., Skrtic, S., Sharer, K., Hill, J. M., Dunbar, C. E., Koretsky, A. P. (2004) MRI detection of single particles for cellular imaging. *Proc. Natl Acad. Sci. USA* **101**: 10901–10906

Silva, A. C., Kim, S. G., Garwood, M. (2000) Imaging blood flow in brain tumors using arterial spin labeling. *Magn. Reson. Med*. **44**: 169–173

Soule, B. P., Hyodo, F., Matsumoto, K., Simone, N. L., Cook, J. A., Krishna, M. C., Mitchell, J. B. (2007) The chemistry and biology of nitroxide compounds. *Free Radic. Biol. Med*. **42**: 1632–1650

Stratford, I. J., Adams, G. E., Bremner, J. C., Cole, S., Edwards, H. S., Robertson, N., Wood, P. J. (1994) Manipulation and exploitation of the tumour environment for therapeutic benefit. *Int. J. Radiat. Biol*. **65**: 85–94

Subramanian, S., Matsumoto, K., Mitchell, J. B., Krishna, M. C. (2004) Radio frequency continuous-wave and time-domain EPR imaging and Overhauser-enhanced magnetic resonance imaging of small animals: instrumental developments and comparison of relative merits for functional imaging. *NMR Biomed*. **17**: 263–294

Swartz, H. M. (1990) Principles of the metabolism of nitroxides and their implications for spin trapping. *Free Radic. Res. Commun*. **9**: 399–405

Swartz, H. M., Sentjurc, M., Morse, P. D. (1986a) Cellular metabolism of water-soluble nitroxides: effect on rate of reduction of cell/nitroxide ratio, oxygen concentrations and permeability of nitroxides. *Biochim. Biophys. Acta* **888**: 82–90

Swartz, H. M., Chen, K., Pals, M., Sentjurc, M., Morse, P. D. (1986b) Hypoxia-sensitive NMR contrast agents. *Magn. Reson. Med*. **3**: 169–174

Torigian, D. A., Huang, S. S., Houseni, M., Alavi, A. (2007) Functional imaging of cancer with emphasis on molecular techniques. *CA Cancer J. Clin*. **57**: 206–224

Utsumi, H., Yamada, K. (2003) In vivo electron spin resonance-computed tomography/nitroxyl probe technique for non-invasive analysis of oxidative injuries. *Arch. Biochem. Biophys*. **416**: 1–8

Yamada, K. I., Kuppusamy, P., English, S., Yoo, J., Irie, A., Subramanian, S., Mitchell, J. B., Krishna, M. C. (2002) Feasibility and assessment of non-invasive in vivo redox status using electron paramagnetic resonance imaging. *Acta Radiol*. **43**: 433–440

Yu, N. Y., Brown, J. M. (1984) Depletion of glutathione in vivo as a method of improving the therapeutic ratio of misonidazole and SR 2508. *Int. J. Radiat. Oncol. Biol. Phys*. **10**: 1265–1269

Yuhas, J. M. (1983) Efficacy testing of WR-2721 in Great Britain: everything is black and white at the gray lab. *Int. J. Radiat. Oncol. Biol. Phys*. **9**: 595–598